

## 3-dimensional anisotropic thermal transport in microscale poly(3-hexylthiophene) thin films

Xuhui Feng<sup>a</sup>, Guoqing Liu<sup>a</sup>, Shen Xu<sup>a</sup>, Huan Lin<sup>a</sup>, Xinwei Wang<sup>a,b,\*</sup>

<sup>a</sup> Department of Mechanical Engineering, 2010 Black Engineering Building, Iowa State University, Ames, IA 50011, USA

<sup>b</sup> School of Environmental and Municipal Engineering, Qingdao Technological University, Qingdao, Shandong 266033, PR China

### ARTICLE INFO

#### Article history:

Received 7 December 2012

Accepted 27 January 2013

Available online 6 February 2013

#### Keywords:

P3HT

Thermal conductivity

Anisotropy

### ABSTRACT

Anisotropy in material structure leads to distinct anisotropy in mechanical and thermal properties for polymer materials. In this work, poly(3-hexylthiophene) (P3HT) thin films are fabricated using the spin coating technique for investigation of anisotropic thermal transport. Raman spectroscopy study of spin-coated P3HT films confirms the partially aligned molecular structure. Based on the main orientation of molecular chains, 3-dimensional thermal characterization is performed to understand the anisotropic thermal transport. The thermal conductivity varies from 0.1 to 3.18 W/m K and presents strong orientation-dependent feature. The anisotropy factor for in-plane thermal conductivity spans in the range of 2–4, lower than the factor for perfectly aligned structure. For thermal diffusivity, strong anisotropy is also observed. Particularly, for the out-of-plane direction, the thermal diffusivity is found almost one order of magnitude lower than that in the in-plane direction.

© 2013 Elsevier Ltd. All rights reserved.

### 1. Introduction

As a promising polymer material, poly(3-hexylthiophene) (P3HT) can release free electrons and therefore embraces advantage like semiconductors. In addition, more advantages over conventional semiconductors are observed with P3HT, such as light weight, processability and environmental sustainability. Therefore P3HT has attracted tremendous attention from scientists and researchers in the past. Large collections of achievements have been reported regarding its novel structures and properties [1]. Various forms of P3HT materials have been synthesized for research and industrial applications, such as thin films [2–9], microwires [4,9,10] and nanofibers [9,11–16]. Because of its special electrical, optical and thermal properties, P3HT has been broadly adopted in applications such as photovoltaic cells, gas sensors, field-effect transistors and many other fields [1]. To determine the density of P3HT film, atomic force microscopy (AFM) analysis in combination with Rutherford backscattering spectroscopy data was applied and the density is estimated around  $1.33 \pm 0.07 \text{ g/cm}^3$  [2]. Thermal behavior and morphology transition of P3HT thin films developed by spin-casting was studied by Hugger et al. [3] using X-ray diffraction measurement with the AFM data. The transition

temperature was found about 225 °C after which a layered and smectic liquid crystalline phase of P3HT formed. The intrinsic photoconductivity of P3HT polymers was measured and conclusion was made that higher mobility is associated with higher molecular weight using optical pump-THz probe spectroscopy [5]. The molecular structure of P3HT has been studied [17] and the result indicated that rotation of the planes containing the conjugated rings in P3HT substantially contributed to electrical conductance: the rotation reduces the electron and hole bandwidths and opens up the energy gap between occupied and empty states.

For P3HT films, of particular interest is the often strong anisotropy caused by molecular structures. Fabrication processes such as spin-coating and stretching/drawing could yield highly aligned molecular structures along the deformation direction, and consequently yield highly anisotropic properties, for instance, the thermal properties that we report in this work. Study of anisotropy has already been conducted on numerous polymers. Models by Henning [18] and Hansen [19] were proposed to account for the impact of molecule orientation on the thermal transport in amorphous polymers. For semicrystalline polymers, the molecular alignment can result in larger anisotropy than that in fully-amorphous polymers. Choy's model [20] to study the anisotropic thermal transport in polymer material adopted the thermal conductivity of crystallite perpendicular and parallel to molecular orientations, along with geometrical definition for the orientation of the crystallite and drawing direction. Experimental investigations of the anisotropic heat conduction in stretched

\* Corresponding author. Department of Mechanical Engineering, 2010 Black Engineering Building, Iowa State University, Ames, IA 50011, USA. Tel.: +1 515 294 2085; fax: +1 515 294 3261.

E-mail address: [xwang3@iastate.edu](mailto:xwang3@iastate.edu) (X. Wang).

polymers have been conducted by several groups. Kilian and Pietralla [21] measured the dependence of anisotropy factor of thermal diffusivity for uniaxially stretched polyethylene. Results showed that the intrinsic anisotropy factor ranges from about 2 for completely amorphous structure to about 50 for completely crystalline polymers. Rantala [22] measured the anisotropic ratio of thermal conductivity of plastic foils whose thicknesses were about 30–100  $\mu\text{m}$  and draw ratio from about 2 to 8. The determined anisotropic ratios vary in a small range of 1–2. Piraux's work [23] proved that for highly orientated structures, the thermal conductivity is enhanced by 15–60 times higher than that of non-orientated polyacetylene. Choy et al. [24] developed a pulsed photothermal radiometry technique by combining a line-shaped laser beam with the laser-flash radiometry method. This technique is able to measure the thermal conduction behavior for biaxially stretched polymer films. A polyethylene film with a draw ratio of 200 was measured and the anisotropy of thermal diffusivity was determined to be even greater than 90. Kurabayashi's work [25] presented three techniques to examine the vertical and lateral thermal conduction in polymer films on a substrate. Data reported indicates that the lateral thermal conductivity is larger by a factor of six than the effective vertical thermal conductivity when the film thickness varies between 0.5 and 2.5  $\mu\text{m}$ . The Harmonic joule heating technique [26,27] was employed to study the anisotropic thermal conductivity of dielectric films. This technique employs metal lines that serve as both heater and thermometer. The lateral spreading of heat inside the film changes the one-dimensional temperature field to achieve the purpose of measuring anisotropic thermal conductivity. For solution-cast P3HT films, the temperature dependence of anisotropic conductivity was investigated by Liu et al. [28]. Their results indicate the electrical conductivity in the perpendicular direction increases with increasing temperature while the electrical conductivity along the parallel direction decreases greatly after 50 °C. This change is attributed to structural anisotropy variation with temperature change. The thermoreflectance imaging technique [29] with localized heat source provides an instant and detailed description of the 2-dimensional thermal map of area surrounding the heat source. It is valid for materials with either isotropic or anisotropic in-plane/out-of-plane thermal conductivity in thin films.

Different synthesis methods for P3HT films, such as solvent casting and spin coating, are widely used to produce P3HT thin film [3]. In solution-cast thin films, P3HT forms needle or plate like crystallites oriented with respect to the substrate, while in spin-coated P3HT films, non-equilibrium structures with reduced order and orientation is always displayed. In this work, free-standing spin-coated P3HT thin film is fabricated for anisotropic thermal transport investigation. Two transient techniques are applied for thermal characterization. The pulsed laser-assisted thermal relaxation 2 (PLTR2) technique [30], which is capable of characterizing both in-plane and out-of-plane thermal transport, is used to measure the 3-dimensional (3D) anisotropic thermal properties. Another technique, transient electrothermal (TET) [31,32] technique is used as a validation of the results from PLTR2. In addition, the TET technique could be used to determine the anisotropic thermal conductivity. The TET technique has been used in our group to investigate the thermophysical properties of P3HT films fabricated from solution with different concentrations of P3HT content [32]. Concentration of P3HT content in the solution not only impacts the thickness of the spin-coated thin film, it also strongly influences the thermophysical properties. In this work the concentration of P3HT content in the solution is fixed at 2%, in order to keep the thickness of P3HT film to be around a few tens of microns, and also to eliminate irrelevant impact on thermal properties. In Section 2, synthesis of P3HT thin films is introduced followed by physical

principles of 3D characterization of thermal transport using the PLTR2 and TET techniques. Experimental results and discussions are presented in Section 3 to show the anisotropy factor and relevance between structural anisotropy and thermal properties of P3HT thin films. Measurement uncertainty and radiation effect is also analyzed in Section 3.

## 2. Materials and methods

### 2.1. Sample preparation

Regioregular P3HT (average molecular weight = 50,000 MW) is purchased from Rieke Metals and anhydrous chloroform is purchased from Sigma Aldrich. As-purchased compounds are used without further processing or purification. The preparation of P3HT solution is conducted in an argon glove compartment in order to eliminate potential danger to human body. After adding the P3HT into chloroform, the solution is then magnetically stirred in a capped vial for about 1 h, with auxiliary heating at 50 °C to help dissolve. The P3HT thin film is fabricated in open air using spin-coating, at 4500 rpm for 25 s in a Pyrex glass dish. Because of the strong centrifugal force in the spin coating process, P3HT molecular chains will be stretched following certain orientations. The main orientations can somewhat be distinguished from the surface pattern of spin-coated P3HT thin film. In order to better define and interpret the 3D anisotropic thermal transport in the spin-coated film, a small rectangular-shaped portion of the P3HT film is selected and the P3HT molecular chains alignment is sketched to present interior structural anisotropy in Fig. 1. A truth worth of attention is that the main structural feature of P3HT is a layered structure, in which P3HT molecular chains are laterally packed and separated by the side chains [3]. Therefore the orientation of P3HT main chains is completely in each plane and little interaction exists along out-of-plane direction, as shown by the layered structure in Fig. 1(a). A Cartesian coordinate system is introduced and the axes of the coordinate system are used to represent parallel to alignment direction ( $x$ -axis), in-plane perpendicular to alignment direction ( $y$ -axis) and out-of-plane direction ( $z$ -axis). Thermal transport in the rectangular-shaped piece is then distinguished and characterized referring to these three directions. For direction parallel to the orientation ( $x$ -axis), thermal properties are marked with subscript '||', while for direction that is in-plane but perpendicular to orientation ( $y$ -axis), it is expressed as ' $\perp$ , in'. The out-of-plane direction ( $z$ -axis) is obviously also perpendicular to the orientation and is defined with subscript ' $\perp$ , out'. Atomic force microscopy is applied to study the topography of the spin-coated film. Images at different scales [Fig. 1(b)] show that no evident microstructure is observed. Also the surface of the film is quite flat. The initial state of P3HT film as obtained from spin coating is amorphous and the crystallinity is very low. Annealing is expected to assist transition to higher crystallinity and better alignment [3]. In this work, our study is focused on as-prepared P3HT films. The effect of annealing on thermal transport and anisotropy will be investigated in the near future.

The thickness of spin-coated thin film is substantially dependent on the concentration of P3HT content in solution [3,32]. The thickness of spin-coated P3HT films in this work is controlled to be around 11–35  $\mu\text{m}$ . Due to its poor electrical conductivity, the spin-coated P3HT thin film needs to be coated with gold film to enhance both the conduction of electrical current and the absorption of laser irradiation. The coating process is performed using Denton Desk V sputter coater and both sides of the P3HT thin film are coated to fulfill different purposes. The configuration of the coated layer is presented in Fig. 2. The rear side is coated from end to end for 40 s ( $\sim 20$  nm) and is in direct contact with aluminum electrodes

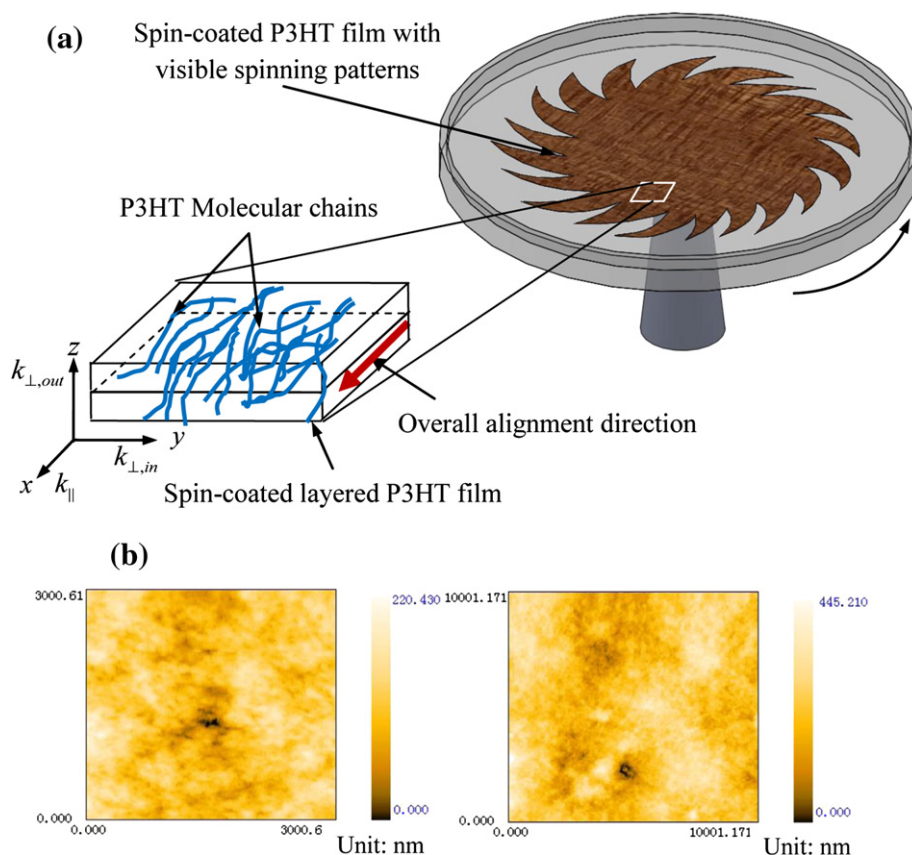


**Fig. 1.** (a) A schematic of the molecular structure within P3HT thin films. The coordinate system is shown to demonstrate the definition of 3D anisotropy regarding the orientation of P3HT molecular chains. An arrow is used to show the approximate overall alignment direction. (b) AFM images of spin-coated P3HT film as prepared at  $3 \times 3 \mu\text{m}$  (left) and  $10 \times 10 \mu\text{m}$  (right) scales.

surface to ensure electrical conduction. The front side is only coated in a limited area for 80 s ( $\sim 40 \text{ nm}$ ) and the gold film is not in contact with the silver paste. The purpose for the gold film on the front side is for absorption of laser irradiation. The total thickness of the coated gold film is around 120 nm and is very small compared to the thickness of P3HT film ( $\sim 11\text{--}35 \mu\text{m}$ ). The impact from gold coating on measured results will be further discussed in Section 3.

## 2.2. Experimental principle for characterizing 3D anisotropic thermal transport

During spin coating, molecule chains are mostly oriented along the draw direction and monomers in each chain are bonded by strong covalent force. In the direction perpendicular to the orientation, only relatively weak interaction via Van der Waals force or H-bond exists among the molecular chains. In addition, because the spin-coating process squeezes the P3HT molecular chains to mainly distribute within a thin plane and also stacks these planes into a layered structure, out-of-plane interactions among P3HT molecular chains is expected to be the weakest because that main chains are separated by side chains and therefore the contact of main chains along this direction is minimal. This strong anisotropy in structure leads to substantial anisotropic thermal transport in spin-coated P3HT thin films. Techniques to characterize the thermal transport in each direction drastically differ depending on the dimension and thermal transport inside [33].

Two transient techniques are employed in this work to characterize the anisotropic thermal transport in P3HT thin films. The PLTR2 technique (shown in Fig. 2), which is improved on the PLTR

technique [30], is capable of simultaneously determining thermal properties along both in-plane and out-of-plane directions based on one measurement. This technique consists of the flash technique [34] with one distinct modification: a constant DC current is fed through the back film to sense the temperature change, instead of using an infrared detector to probe temperature rise on the rear surface. The amplitude of the DC current is controlled to cause negligible joule heating. Resistance change of the gold film on the back side is used to depict temperature change and to consequently determine thermal properties. A schematic of PLTR2 is shown in Fig. 2. The gold film on top surface is for absorption of laser beam. Absorbed laser energy excites the electrons in neighboring thin layer. Due to the relatively small electronic heat capacity, the electron temperature increases fast and then hot electrons interact with lattice in the gold layer through scattering, causing the temperature of the whole gold layer to rise immediately. Thermal energy then transfers from the top gold layer to P3HT film. This out-of-plane thermal transport completes in an extremely fast manner like hundreds of microseconds. Parker [34] analytically solved the theoretical temperature distribution along the thickness direction and the thermal diffusivity is derived as

$$\alpha = 1.38D^2/\pi^2t_{1/2}, \quad (1)$$

where  $t_{1/2}$  is the time taken to reach half of the maximum temperature rise at the back of the sample and  $D$  is the thickness of the P3HT thin film.

The out-of-plane thermal transport is followed by a relatively slow in-plane thermal decay due to the dissipation of thermal

energy to electrodes. Because the length of thin film is significantly greater than thickness, the physical model for thermal decay is simplified as one-dimensional (along the length direction of the film). The governing equation of this one-dimensional heat diffusion is,

$$\frac{\partial(\rho c_p T)}{\partial t} = k \frac{\partial^2 T}{\partial x^2} + q_0, \quad q_0 = \begin{cases} q_{\text{laser}} + q_{\text{joule}}, & 0 \leq t \leq \Delta t \\ q_{\text{joule}}, & t > \Delta t \end{cases}, \quad (2)$$

where  $q_0$  includes both joule heating and laser pulse heating,  $k$ ,  $\rho$ , and  $c_p$  are the thermal conductivity, density, and specific heat of the sample. Because the joule heating introduced by the constant DC current is relatively weak and contributes to steady temperature distribution during the process, only laser pulse heating is considered in theoretical study.  $\Delta t$  is the laser pulse width and the laser intensity is assumed to be constant during  $\Delta t$  ( $\sim 7$  ns). This laser heating time is significantly smaller than characteristic time of heat diffusion in film. In practice, the laser beam has Gaussian distribution in space. To suppress the spatial non-uniformity, the laser beam spot ( $\sim 8$  mm) is chosen to be larger than the length of film ( $\sim 3$  mm), ensuring an uniform laser intensity distribution over the film surface. Equation (2) can be solved using Green's function and more details can be referred to another work [30] in our group. Only the analytical solution is presented here for analysis. Integration of the solution  $T(x, t)$  along the length direction gives the temporal temperature variation,

$$\begin{aligned} \bar{T}(t) &= \frac{1}{L} \int_{x=0}^L T(x, t) dx \\ &= \begin{cases} \frac{8q_{\text{laser}}L^2}{k\pi^4} \sum_{m=1}^{\infty} \frac{1 - \exp[-(2m-1)^2\pi^2\alpha t/L^2]}{(2m-1)^4} & (0 < t \leq \Delta t) \\ \frac{8q_{\text{laser}}L^2}{k\pi^4} \sum_{m=1}^{\infty} \frac{\exp[-(2m-1)^2\pi^2\alpha t/L^2] \{ \exp[(2m-1)^2\pi^2\alpha\Delta t/L^2] - 1 \}}{(2m-1)^4} & (t > \Delta t) \end{cases}, \end{aligned} \quad (3)$$

where  $L$  is the sample length, and  $\alpha$  thermal diffusivity. Since only the temperature decay after laser heating is our interest, the solution for time larger than  $\Delta t$  is considered. In addition, the pulse width  $\Delta t$  is only a few nanoseconds and further simplifications are made to give a normalized temperature distribution for the thermal decay process,

$$T^* = \frac{8}{\pi^2} \sum_{m=1}^{\infty} \frac{\exp[-(2m-1)^2\pi^2\alpha t/L^2]}{(2m-1)^2}. \quad (4)$$

This equation demonstrates that for any material with an arbitrary length, the normalized temperature relaxation follows the same profile with respect to the Fourier number  $Fo$  ( $=\alpha t/L^2$ ). The thermal diffusivity is varied to fit the normalized experimental temperature rise, and the value giving the best fit is taken as the thermal diffusivity of the P3HT film.

The TET technique [31,32] has been widely applied in our lab to characterize the thermal properties of various film structures, such as P3HT thin film [32] and  $\text{TiO}_2$  thin film [35]. Compared to PLTR2, TET technique is mostly applied to investigate in-plane thermal transport and is capable of determining the thermal conductivity,

too. In this study, the TET technique is employed to acquire in-plane thermal diffusivity of P3HT films as validation of that from PLTR2. The experimental principle of the TET technique is presented in Fig. 2 as well. During the TET experiment, a step DC current ( $I$ ) is fed through the P3HT thin film to introduce joule heating. Transient temperature increase of the P3HT thin film is strongly dependent on the heat transfer within the film. Temperature change then leads to resistance change and consequently induces an overall voltage change. An oscilloscope is used to record the voltage change of the P3HT thin film for further data analysis. The supplied current–time ( $I$ – $t$ ) profile and induced voltage–time ( $U$ – $t$ ) profile recorded by the oscilloscope is also presented in Fig. 2. As explained in this figure, under the feeding of a square current (red dashed line), the induced voltage profile (black solid line) undergoes a transient increase and then reaches the steady state, indicating that thermal equilibrium is achieved. The transient phase can be used to determine the thermal diffusivity, while the voltage difference between initial and steady states helps to determine the thermal conductivity. Under the experimental conditions in this work, the physical model of the TET technique is simplified into a one-dimensional heat transfer model and more details can be referred to our previous work [35]. The normalized transient temperature increase ( $T^*$ ) is solved as,

$$T^* = \frac{96}{\pi^4} \sum_{m=1}^{\infty} \frac{1 - \exp[-(2m-1)^2\pi^2\alpha t/L^2]}{(2m-1)^4}. \quad (5)$$

The voltage evolution ( $V_{\text{film}}$ ) recorded by the oscilloscope is directly related to the average temperature change of the P3HT thin film as,

$$V_{\text{film}} = IR_0 + I\eta \frac{8q_0L^2}{k\pi^4} \times \sum_{m=1}^{\infty} \frac{1 - \exp[-(2m-1)^2\pi^2\alpha t/L^2]}{(2m-1)^4}, \quad (6)$$

where  $V_{\text{film}}$  is the recorded overall voltage of the P3HT thin film,  $I$  the current passing through the sample,  $R_0$  the resistance of P3HT thin film before heating, and  $\eta$  temperature coefficient of electrical resistance. It is obvious that the measured voltage change is inherently related to the temperature change of the P3HT thin film. By globally fitting the theoretical solution to the experimental data using the least square method, the value that gives the best fitting results is the in-plane thermal diffusivity of the sample. From the derivation of theoretical solution for this one-dimensional heat transfer problem, it is also feasible to derive the thermal conductivity based on the temperature difference between starting point and steady state,  $\Delta T$ . With a calibration process to determine the temperature coefficient of resistance  $\eta$ , the temperature change  $\Delta T$

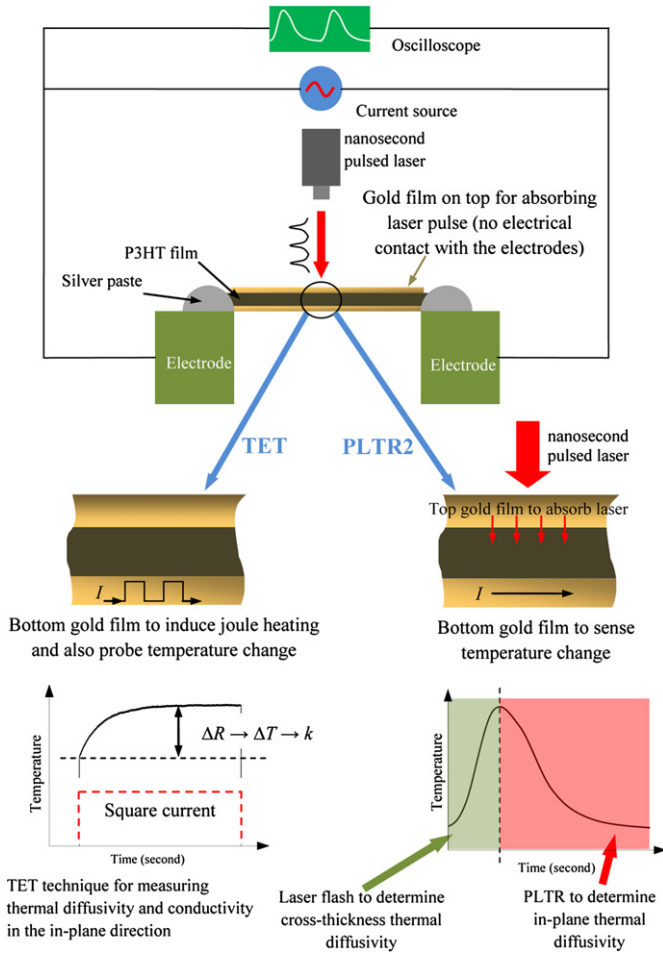


**Fig. 2.** Experimental schematic and principle (not to scale) for applying TET and PLTR2 techniques to characterize 3D anisotropic thermal transport in P3HT thin films.

is calculated with known  $\Delta R$  and then the thermal conductivity is obtained as  $I^2RL/(12A\Delta T)$ .

As discussed before, the P3HT film is pre-coated with gold to ensure electrical conducting and optical energy absorption. Therefore, the determined thermal properties are still effective values that comprise contribution from the gold film. A methodology to exclude the influence of gold is introduced elsewhere [35]. The thermal transport effect caused by the coated layer can be subtracted using the Lorenz number without increasing the uncertainty. The intrinsic thermal diffusivity ( $\alpha$ ) of the P3HT thin film in the in-plane direction is determined as

$$\alpha = \alpha_{\text{eff}} - \frac{L_{\text{Lorenz}}TL}{RA_w\rho c_p}, \quad (7)$$

in which  $\rho$  and  $c_p$  are the effective density and specific heat of the sample,  $A_w$  the cross-sectional area of the film, and  $L_{\text{Lorenz}}$  the Lorenz number of gold. Because of the specialty with gold film coated over P3HT film, the  $R$  should be effective resistance of all gold layers. The actual thermal conductivity ( $k$ ) can also be determined following the similar methodology as,

$$k = k_{\text{eff}} - \frac{L_{\text{Lorenz}}TL}{RA_w}. \quad (8)$$

In order to practically determine the actual thermal diffusivity and thermal conductivity, physical parameters such as density and

specific heat are required, besides the effective thermal parameters, dimensional parameters and temperature. The effective volume-based specific heat  $\rho c_p$  is calculated based on the definition of thermal diffusivity,  $\alpha = k/\rho c_p$ , after determining the effective thermal parameters experimentally. With real thermal properties, the density of P3HT thin film is then derived without influence from the gold film. More details regarding this modification to derive actual values will be demonstrated in the following section. After obtaining the actual thermophysical properties based on the modifications, another factor needs to be considered. Although the whole experiment is conducted at vacuum condition around 1 mTorr, the real situation would be complicated and pressure level may be higher than that due to vacuum gauge reading error. Therefore the heat conduction induced by gas in the vacuum chamber brings effects to the actual results. A calibration process using a standard material (glass fiber) is performed to derive the contribution of gas conduction and it is then used to further modify the determined thermophysical properties of P3HT thin films.

### 3. Results and discussion

#### 3.1. Anisotropic thermal characterization

In this section, one P3HT thin film is particularly selected to demonstrate the anisotropic thermal characterization process and post data analysis using both PLTR2 and TET techniques. The length, width and thickness of this P3HT sample are 4.52 mm, 0.501 mm and 20  $\mu\text{m}$ , respectively. The experimental setup for PLTR2 can be referred to Fig. 2. A pulsed Nd:YAG laser (Quanta-Ray) of 1064 nm wavelength is utilized to provide pulsed laser irradiation. Temporal span of each pulse is about 6–8 ns and the energy is about 200 mJ. The laser beam spatially obeys Gaussian distribution and the size of beam spot is about 8 mm. It is much larger than the P3HT film length, which is around 2–4 mm. Size comparison between laser beam spot and P3HT film supports the assumption made in PLTR2 analytical model that the film receives uniform laser irradiation. A constant DC current provided by a current source (Keithley 6221) is fed through the film during the whole measurement. Magnitude of the DC signal is carefully selected to ensure both appreciable voltage signal level and minimum joule heating. An oscilloscope (Tektronix TDS 7054 digital phosphor oscilloscope) is connected to the film to record voltage variation for data analysis. As seen in Fig. 2, the recorded voltage profile contains information for determining both in-plane and out-of-plane thermal properties. In Fig. 3(a), for the selected P3HT thin film, fitting profile of thermal decay for deducing in-plane thermal diffusivity is presented and the thermal diffusivity is determined at  $4.66 \times 10^{-6} \text{ m}^2/\text{s}$ . By varying the value of thermal diffusivity, the uncertainty of the in-plane thermal diffusivity is estimated at 10% using the PLTR2 technique when distinct deviation is observed. For the out-of-plane thermal diffusivity, it is calculated directly based on the rapid temperature rise under laser irradiation, as shown in Fig. 3(b). The time to reach half of the maximum temperature rise,  $t_{1/2}$ , is determined from this graph and then is used to calculate the out-of-plane thermal diffusivity using Eq. (1). However, as observed in this graph, the temperature rise profile is not smooth and contains oscillation in data. Further examination shows that the voltage increase is just slightly greater than 1.5 mV. Based on the laser flash theory, thermal excitation is applied on the front surface and consequent temperature increase on the rear surface is probed for analysis. However, the maximum surface temperature rise of front surface under laser irradiation is estimated to be tens of times greater than the maximum temperature rise at the rear surface. In order to induce an appreciable temperature change at the rear surface, the laser energy exerted on front surface of the P3HT film

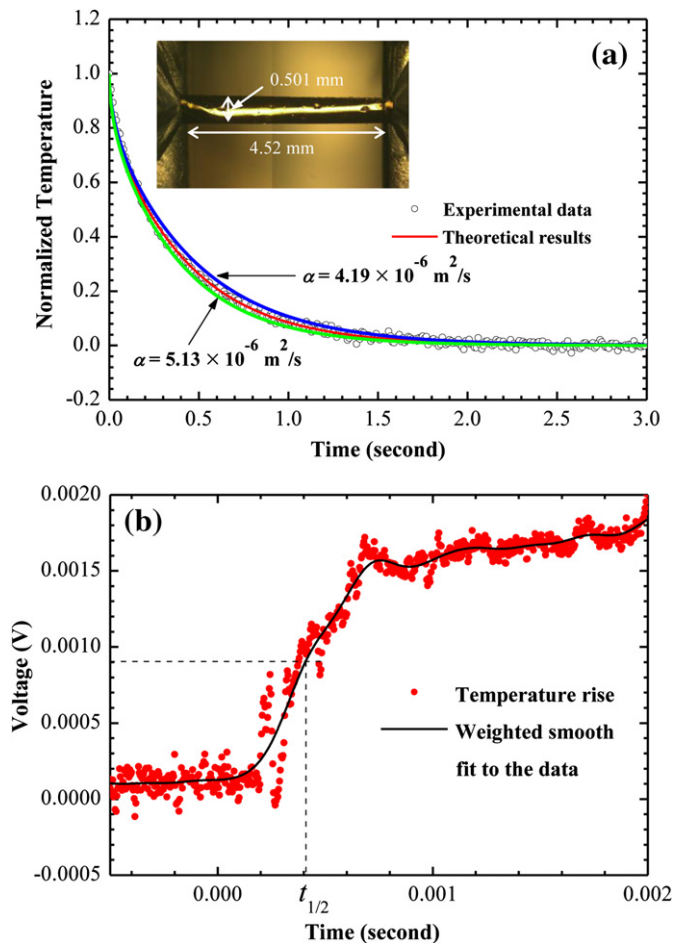


**Fig. 3.** (a) Comparison between theoretical results and experimental data for a selected P3HT film to determine the in-plane thermal diffusivity using the PLTR2 technique, while a microscopic image is shown in the inset for the sample connected between two electrodes. The length, width and thickness of this film are 4.52 mm, 0.501 mm and 20.0  $\mu\text{m}$ , respectively. (b) temperature rise curve at the back of the film due to pulsed laser irradiation.

needs to be strong but destruction may probably be caused to the film. To keep the sample intact and achieve sensible signal, laser energy and probing DC current have to be selected carefully to acquire the best voltage signal. Although the profile in Fig. 3(b) still has obvious noise, it is good enough for determination of out-of-plane thermal diffusivity. Further analysis using weighted smooth algorithm to fit original data helps determine an accurate value of  $t_{1/2}$ . The out-of-plane thermal diffusivity  $\alpha_{\perp, \text{out}}$  characterized using this strategy is determined to be  $2.14 \times 10^{-7} \text{ m}^2/\text{s}$ , about one order of magnitude lower than that of the in-plane direction.

Different from the PLTR2 technique using laser irradiation, the TET technique applies electrical current as a source of thermal excitation and measures in-plane thermal properties only. Experiment setup of the TET technique is similar to that of PLTR2 as shown in Fig. 2, except that laser apparatus is no longer required. The same current source (Keithley 6221) is used, but to supply a step current and the voltage response is recorded by the high-speed oscilloscope (Tektronix TDS 7054 digital phosphor oscilloscope). Least square fitting results for the TET data is shown in Fig. 4(a) and the in-plane thermal diffusivity is determined at  $4.73 \times 10^{-6} \text{ m}^2/\text{s}$ . The same strategy by altering the thermal diffusivity to observe appreciable deviation from the experimental data is used to determine the uncertainty of the TET

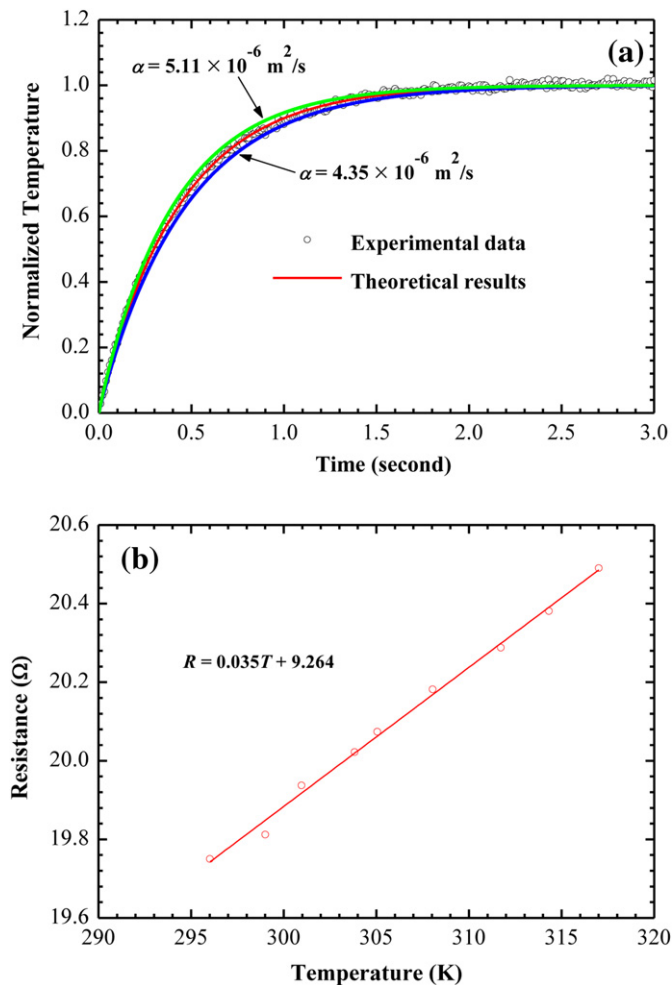


**Fig. 4.** (a) Comparison between theoretical solution and experimental data for P3HT thin film using TET technique and (b) linear fitting graph of temperature coefficient of resistance for P3HT thin film.

measurement. Uncertainty for the thermal diffusivity from TET measurement is about 8%. Comparison between the in-plane thermal diffusivity determined by TET and PLTR2 suggests that the in-plane thermal diffusivity is determined with high credibility, with only about 1.5% difference between these two techniques. From the voltage–time profile in the TET experiment, the thermal conductivity is further calculated with the calibration data of temperature coefficient of resistance. During calibration, a heating plate is used to provide the heated environment and a thermocouple is closely attached to the P3HT film, ensuring that the thermometer reading can accurately reflect the temperature of the film. A digital multimeter (Agilent 34401A) is connected to monitor the resistance change. The heating and the consequent temperature rise range are controlled moderate to assure the intactness of P3HT thin films [35]. The calibration profile of this selected P3HT thin film is shown in Fig. 4(b). Distinct linear temperature–resistance relationship similar to metallic materials is observed and the resistance is contributed by the gold film, which strongly enhances the electrical conduction of the film. The temperature coefficient of resistance is determined at  $3.54 \times 10^{-2} \text{ } \Omega/\text{K}$  for this film. With 14 mA DC current passing through the film, the resistance change is calculated to be 1.36  $\Omega$  and the resulting temperature rise is 38.4 K. The thermal conductivity is then calculated as 3.98 W/m $\cdot$ K.

So far the thermal properties determined above using TET and PLTR2 are effective values, containing impacts from various aspects. The first impact to measurement uncertainty is the conduction of heat by remaining gas in the vacuum chamber since it is not absolutely zero pressure during the measurement and calibration. During the TET and PLTR2 measurement and calibration, the pressure within the vacuum chamber is 94, 56, and 10 mTorr, respectively. The effect of the gas conduction on the thermal diffusivity can be expressed as  $hP \cdot L^2 / [A_w \pi^2 (\rho c_p)_e]$ , where  $h$  is the effective heat conduction coefficient by the gas,  $P$  the sample's perimeter in the length direction, and  $A_w$  sample cross-sectional area. We have conducted calibrations using a reference material (glass fiber) to measure  $h$  under different pressure levels. Based on the respective pressure,  $h$  is determined as 11.15, 6.64, and 1.186 W/m<sup>2</sup> K in TET and PLTR2 measurements and calibration. Accordingly, the effect of gas conduction can be subtracted precisely from the measured thermal diffusivity. During calibration to determine the temperature coefficient of electrical resistance, a coefficient of  $mL / \tanh(mL) [m^2 = hP / (kA_w)]$  should be used to multiply the directly determined thermal conductivity to account for the effect of gas conduction. Details of the rigorous derivation will be published in our later work.

Another important influence is brought in by the gold film. A methodology to subtract the effect of gold film is introduced in the previous section. The effective volume-based specific heat is  $C_{\text{eff}} = k_{\text{eff}} / \alpha_{\text{eff}}$ . After modifying the effective thermal properties by considering the gas effect, the effective volume-based specific heat can be determined to be  $0.82 \times 10^6$  J/m<sup>3</sup> K, using the relationship introduced. Value of Lorenz number used in this work is  $4.9 \times 10^{-8}$  W  $\Omega$ /K<sup>2</sup>, which is chosen considering that the Lorenz number drastically increases with reduced size. For bulk metals, the Lorenz number is  $2.45 \times 10^{-8}$  W  $\Omega$ /K<sup>2</sup>, while for gold film of 10 nm thickness, this value rises to  $7.40 \times 10^{-8}$  W  $\Omega$ /K<sup>2</sup>. Therefore an approximated median for Lorenz number is estimated and used in this work. By subtracting both gas conduction effect and the effect of gold film, the in-plane thermal diffusivity of P3HT thin film is revised as  $2.81 \times 10^{-6}$  m<sup>2</sup>/s for PLTR2 and  $2.25 \times 10^{-6}$  m<sup>2</sup>/s for TET. With the modification to acquire intrinsic values, the influence from gold films is estimated to be about 12%, indicating the gold film does not significantly impact the measurement. In-plane thermal conductivity is modified using Eq. (8) and is calculated as 2.10 W/m K, indicating the impact of gold coating is also small (around 14%). Calorimetric measurements revealed that for regioregular P3HT an endothermic transition from a crystalline to a liquid crystalline state occurs at 210–225 °C [9]. However, because the temperature during the experiment spans around 25–60 °C, the endothermic transition is not considered and the specific heat is around 1550–1620 J/kg K, depending on the instantaneous temperature of the P3HT film [3]. According to Erwin's work [2], the density of P3HT thin film can be derived based on film thickness and the molecular weight of a P3HT monomer. The average density for P3HT thin film has been determined at  $1.33 \pm 0.07$  g/cm<sup>3</sup> by measuring the thickness and combining the Rutherford backscattering spectroscopy data. Nevertheless, in this work the density of P3HT thin film is individually evaluated using the obtained thermal conductivity, thermal diffusivity and specific heat, based on the definition of the thermal diffusivity,  $\alpha = k / \rho c_p$ . The density of the P3HT thin film is calculated to be 555 kg/m<sup>3</sup> for this sample, much lower than the literature value. Considering that spin-coating process induces highly porous structure and the structure changes during film-peeling off the glass dish, the density is reasonably lower than the bulk value.

### 3.2. Anisotropic thermal transport in microscale P3HT films

The thickness of prepared P3HT thin films varies in a range from 11 to 35  $\mu$ m for our measured samples. The thickness measurement

is conducted using a micrometer caliper and the uncertainty is estimated to be around 10% based on multiple measurements. In this part, 3D anisotropy with thermal transport in spin-coated films will be distinguished and studied, along with explanation from structure perspective. During the spin coating process, combination of the quick volatilization of chloroform content and intense centrifugal force has caused visible spinning pattern seen with the spin-coated film [Fig. 1(a)], indicating the existence of particular orientation of molecular chains. Diagnosis of P3HT structure using polarized Raman spectroscopy verifies that distinct orientation exists within the film and the spectra is shown in Fig. 5. The Raman peak at 1448 cm<sup>-1</sup> is related to the C $\alpha$ =C $\beta$  bond of the thiophene rings, while the small peak around 1382 cm<sup>-1</sup> represents C $\beta$ –C $\beta$  bond stretching [36]. By adjusting the angle between polarized laser beam and presumed orientation of molecular chains (C $\alpha$  = C $\beta$  bond), the intensity of peak at 1448 cm<sup>-1</sup> drastically changes. Detailed trend is shown in the inset of Fig. 5. The intensity of peak at 1448 cm<sup>-1</sup> is at the maximum level at 15°. When the angle increases, the intensity accordingly decreases and achieves the minimum level at 90°. This variation profile depicts that there is a direction inside the film along which the Raman spectra give the strongest signal. This direction should be the orientation of aligned P3HT molecular chains. However this profile also explains that the orientation of chains would not be very perfect and only partial alignment is generated because of the quickly drying process of chloroform and contraction of polymer molecular chains.

Different from previous investigation of anisotropy in polymer film, the thermal property along all three directions are studied in this work, as illustrated by the coordinates shown in Fig. 1(a). Investigations along all three directions comprise this 3D characterization of anisotropy in P3HT thin films. The spin-coating process causes the polymer chains to be oriented along a particular direction because of the strong centrifugal force. In addition, the solvent-drying process induces large stress in the film that squeezes the polymer molecular chains into a layered structure of a few micron thickness along the out-of-plane direction. Therefore, the aligned molecular chains exhibit curvature to certain degrees and the curvature mostly exists along the in-plane direction [3]. This anisotropic structure speculation is supported by the thermal conductivity shown in Fig. 6(a). A fact worth of attention is that the thermal conductivity can only be directly measured for parallel and in-plane perpendicular directions because the calibration process is not applicable for out-of-plane direction. However, an indirect

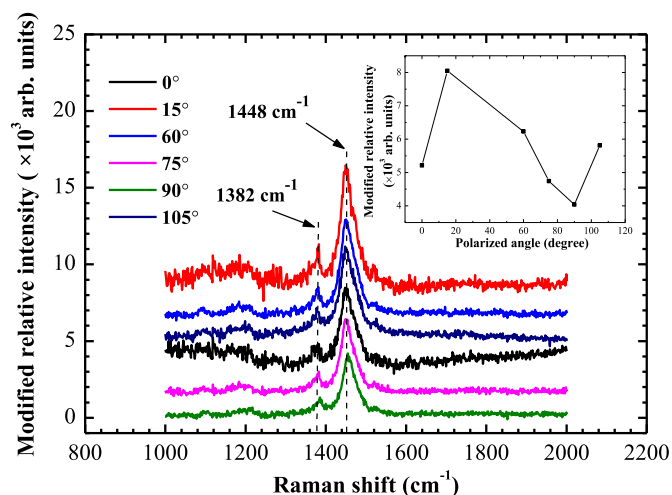


Fig. 5. Raman spectra of P3HT thin film using the polarized laser. Inset graph shows the relation between the maximum intensity and polarized angle.

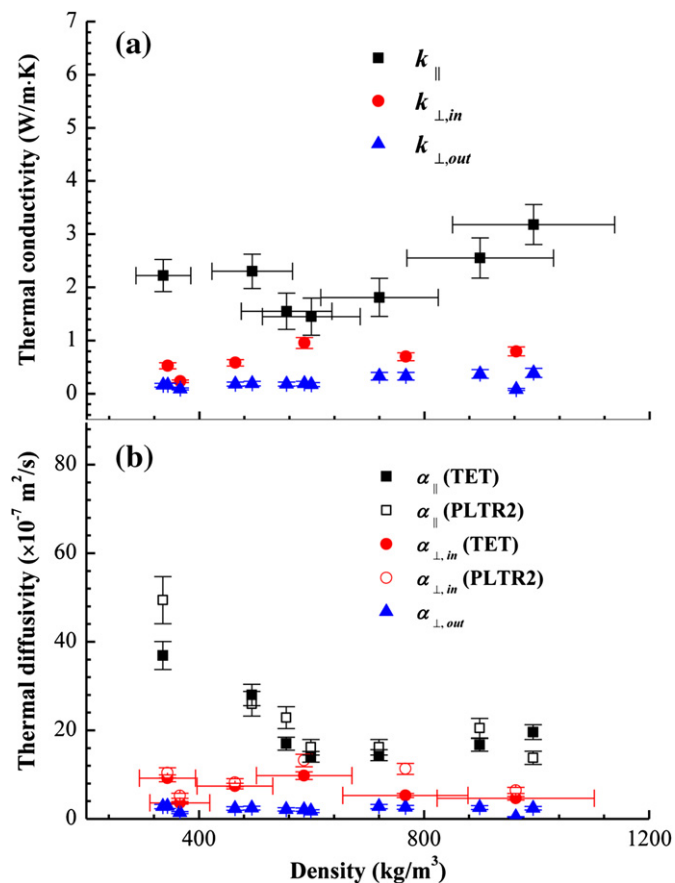


Fig. 6. (a) 3D anisotropic thermal conductivity versus density for all P3HT thin films and (b) 3D anisotropic thermal diffusivity versus the density for all P3HT thin films. Error bars are used to show the uncertainty contained in the results.

method is still feasible to determine the out-of-plane thermal conductivity. With known out-of-plane thermal diffusivity  $\alpha_{\perp, \text{out}}$  and effective volume-based specific heat  $\rho c_p$ , the out-of-plane thermal conductivity can be calculated. In Fig. 6(a), the thermal conductivity versus density of P3HT thin films is shown with error bars. It is observed that appreciable difference emerges between parallel direction thermal conductivity  $k_{\parallel}$  and perpendicular directions  $k_{\perp, \text{in}}$  and  $k_{\perp, \text{out}}$ . For the parallel direction,  $k_{\parallel}$  increases from about 1.45 to 3.18 W/m K. Along the in-plane perpendicular direction, the thermal conductivity is varying around 0.6 W/m K. The values of thermal conductivity are close to the results in our previous work about P3HT thin film [32]. For the out-of-plane direction, the thermal conductivity shows a flat trend around 0.25 W/m K, indicating the weakest coupling of atomic motions along this direction. In addition, the thermal conductivities in parallel and in-plane perpendicular directions present increasing tendency with increasing density. The strong coupling of atomic vibrations by covalent bonds along the molecular chains enhances energy transport and yield more substantial thermal conductivity along chain direction. In contrast, weak Van der Waals interaction between the neighboring chains impedes the transport of lattice vibrations and induces relatively large thermal resistance to heat conduction between chains. For polymer film that embraces perfectly aligned structures, the thermal conductivity anisotropy factor  $k_{\parallel}/k_{\perp, \text{in}}$  is predicted to be greater than  $10^3$  [37]. In this study, the molecular chains in spin-coated film are estimated to be partially aligned as discussed before. Therefore, the thermal conductivity anisotropy factor is in the range of 2–4, much lower than values for perfectly orientated structure.

In Fig. 6(b), thermal diffusivities for both parallel and perpendicular directions for all samples are presented with error bars. Analogous to thermal conductivity, the thermal diffusivity also exhibits distinct anisotropy. Among all three directions, the thermal diffusivity in the out-of-plane direction  $\alpha_{\perp, \text{out}}$ , varies in the range from 1 to  $3 \times 10^{-7} \text{ m}^2/\text{s}$ . These values are about one order of magnitude lower than thermal diffusivities in the other two directions, which are of  $10^{-6} \text{ m}^2/\text{s}$  order. Other than that in the out-of-plane direction, the thermal diffusivity also presents distinguishable anisotropy between parallel and in-plane perpendicular directions. In the parallel direction,  $\alpha_{\parallel}$  changes from 1.40 to  $4.94 \times 10^{-6} \text{ m}^2/\text{s}$ , while in the in-plane perpendicular direction, the thermal diffusivity  $\alpha_{\perp, \text{in}}$  is confined within a lower range from about  $4 \times 10^{-7}$  to  $1.3 \times 10^{-6} \text{ m}^2/\text{s}$ . Dependence of thermal diffusivity on density exhibits opposite tendency compared with the thermal conductivity. Higher density induces lower thermal diffusivity, as observed in our previous work [32] regarding the P3HT film. Thermal conductivity only relies on the densities of phonons and the scattering inside film. Therefore with similar structure, higher density means less cavity and enhanced thermal transport. Nevertheless, the thermal diffusivity is a ratio of material's ability to conduct thermal energy over the capability to store thermal energy. Probably because the effect of density on storing energy is stronger than enhancing thermal transport, the overall effect is that thermal diffusivity decreases with increasing density. Furthermore, as described in the experiment section, PLTR2 and TET techniques are both efficient and precise to characterize anisotropic thermal diffusivity. From Fig. 6(b), thermal diffusivities determined by both techniques are observed to be consistent. The difference  $[(\alpha_{\text{PLTR2}} - \alpha_{\text{TET}})/\alpha_{\text{PLTR2}}]$  based on two sets of results is mostly less than 30%, confirming that the two techniques are capable of characterizing thermal properties and results are obtained with high credibility. A few outliers probably caused by experiment uncertainty are observed.

For uncertainty assessment purpose, error bars are also shown in Fig. 6. As analyzed before in this section, the major contributor to errors is the measurement of dimensions, especially the thickness. Although the deformation caused by micrometer caliper is usually just 1–2  $\mu\text{m}$ , it is not negligible in this experiment because the extremely thin film thickness is only around 11–35  $\mu\text{m}$ . Therefore the maximum measurement uncertainty from the thickness is evaluated to be about 10%. For film length and width, they are read directly from the pictures taken by microscopy and the errors are assumed to be as small as 1%. All experimental devices and equipment, such as the constant current source, oscilloscope and digital multi-meter are calibrated before the measurement. Therefore the uncertainties from current and resistance readings are negligible. From the equation to calculate effective thermal conductivity, the total uncertainty of  $k_{\text{eff}}$  is about 10.1%, demonstrating that the largest uncertainty comes from the measurement of thickness.

For thermal diffusivity, the error is estimated to be 8% for TET technique [Fig. 3(a)] and 10% for PLTR2 [Fig. 4(a)]. These values are determined by changing the thermal diffusivity to examine distinct deviation of the fitting. With effective thermal conductivity and thermal diffusivity, the uncertainty of effective density can also be derived and is estimated to be around 12.9% according to the error propagation theory. After obtaining the errors of all necessary variables, the uncertainties of real thermal diffusivity from TET technique and from PLTR2 are then calculated to be 8.6% and 10.8%, respectively, based on Eq. (7). Uncertainty for real thermal conductivity of P3HT thin films is 10.7% based on Eq. (8), after subtracting the impact from gold film. Then real density of P3HT films is determined from real thermal properties and the error is estimated to be 14.5%. For the out-of-plane direction, the thermal

diffusivity presents relatively stronger noise level and the uncertainty contains contribution from thickness measurement and reading of the parameter  $t_{1/2}$ . It is estimated that errors of out-of-plane thermal diffusivity and thermal conductivity are about 17.3% and 22.0%, respectively. Error bars for thermal properties and density are added in Fig. 6 to present the uncertainties in this experiment.

### 3.3. Impact from radiation heat transfer

Radiation heat transfer from the film surface may be an important issue during the measurement. For radiation heat transfer from film surface, it can be approximated by  $q_{\text{rad}} = \epsilon\sigma A [(T_0 + \Delta T)^4 - T_0^4]$ , where  $\Delta T$  is the average temperature rise over the sample,  $\epsilon$  the surface emissivity,  $\sigma$  the Stefan–Boltzmann constant,  $A$  the effective surface area for radiation heat transfer [=2(W + D)L, W: width, D: thickness, L: length]. Meanwhile, from the expression to calculate thermal conductivity in the TET technique, the heat generation is expressed as  $q_{\text{gen}} = V12k\Delta T/L^2$ , in which  $V$  is the volume of sample and expressed as  $W \cdot D \cdot L$ . This radiation and heat generation estimation is for the steady state of the thin film with a uniform heat generation inside. Although a simple ratio between the radiation heat flow and heat generation cannot precisely represent the experimental case, it provides a sound first-order approximation of the radiation effect. The ratio of radiation to overall heat generation is estimated as,

$$\frac{q_{\text{rad}}}{q_{\text{gen}}} = \frac{\epsilon\sigma \cdot 2(W + D)L \cdot (4T_0^3\Delta T + 6T_0^2\Delta T^2 + 4T_0\Delta T^3 + \Delta T^4)}{\frac{WDL \cdot 12k\Delta T}{L^2}} \times (\Delta T \ll T_0, D \ll W), \quad (9)$$

$$\approx \frac{2\epsilon\sigma T_0^3 L^2}{3kD}$$

At transient state, the ratio is even smaller due to the gradually increasing temperature. For the P3HT thin film, it is estimated that the ratio is less than 1%, by varying the length from 2 mm to 4 mm. In conclusion, the radiation heat transfer in this work is negligible compared to the heat generation and conduction along the sample.

## 4. Conclusion

P3HT thin films were fabricated using the spin coating technique to study the anisotropic thermal transport. Raman spectroscopy study confirmed that the spin-coated P3HT thin films in this work embraced aligned molecular chains and presented strong anisotropy within the structure. By referring to the orientation of the aligned P3HT molecular chains, a 3D characterization system was created to distinguish the thermal transport along three distinct directions: parallel to orientation ( $\parallel$ ), in-plane perpendicular to orientation ( $\perp$ , in) and out-of-plane direction ( $\perp$ , out). The PLTR2 technique, which is capable of studying both in-plane and out-of-plane thermal transport, was employed for 3D characterization of thermophysical properties. As a validation of results from the PLTR2 technique, the TET technique was also used. The thickness of spin-coated P3HT thin film varied from 11 to 35  $\mu\text{m}$ . The measured thermal conductivity and thermal diffusivity both presented strong anisotropy due to the orientation of molecular chains. For thermal conductivity, the anisotropy factor was about 2–4, lower than polymer films that comprise perfectly aligned molecular chains. This anisotropy for thermal conductivity originated from the anisotropy of material structure. Strong covalent bond within the molecular chain strengthens the

phonon transport while the interactions among the chains are much weaker. For thermal diffusivity, same anisotropy was observed in the measured results. Along the out-of-plane direction, the thermal diffusivity was observed to be around 1 to  $2 \times 10^{-7} \text{ m}^2/\text{s}$  and thermal conductivity was just about 0.2 W/m K, almost one order of magnitude lower than the other two directions. This is because the spin coating process squeezed the curved molecular chains into a thin layer of just a few microns. The molecular chains have much less curvatures in the out-of-plane direction. The density of P3HT films was also determined based on the measured thermal diffusivity and conductivity, and was much lower than the literature value, probably due to the highly porous structure formed during the spin coating process.

## Acknowledgment

Support of this work from the Office of Naval Research (N000141210603), Army Research Office (W911NF-12-1-0272), and National Science Foundation (CBET-0931290) is gratefully acknowledged.

## References

- [1] Roncali J. Chem Rev 1992;92(4):711–38.
- [2] Erwin MM, McBride J, Kadavanich AV, Rosenthal SJ. Thin Solid Films 2002; 409(2):198–205.
- [3] Hugger S, Thomann R, Heinzl T, Thurn-Albrecht T. Colloid Polym Sci 2004; 282(8):932–8.
- [4] Kim DH, Park YD, Jang Y, Kim S, Cho K. Macromol Rapid Comm 2005;26(10): 834–9.
- [5] Esenturk O, Melinger JS, Heilweil EJ. 2007 conference on lasers & electro-optics/quantum electronics and laser science conference (CLEO/QELS 2007), vol. 1–5; 2007. p. 2743–4.
- [6] Janssen G, Aguirre A, Goovaerts E, Vanlaeke P, Poortmans J, Manca J. Eur Phys J Appl Phys 2007;37(3):287–90.
- [7] Khaliq A, Xue FL, Varahramyan K. Microelectron Eng 2009;86(11):2312–5.
- [8] Scavia G, Porzio W, Destri S, Schieroni AG, Bertini F. E-Polymers 2009;1–9.
- [9] González R, Pinto NJ. Synth Met 2005;151(3):275–8.
- [10] Kim DH, Han JT, Park YD, Jang Y, Cho JH, Hwang M, et al. Adv Mater 2006; 18(6):719–23.
- [11] Savenije TJ, Kroeze JE, Yang XN, Loos J. Thin Solid Films 2006;511:2–6.
- [12] Laforgue A, Robitaille L. Synth Met 2008;158(14):577–84.
- [13] Kuo CC, Wang CT, Chen WC. Macromol Symp 2009;279(1):41–7.
- [14] Lee S, Moon GD, Jeong U. J Mater Chem 2009;19(6):743–8.
- [15] Pinto NJ, Carrasquillo KV, Rodd CM, Agarwal R. Appl Phys Lett 2009;94(8): 083504.
- [16] Lee SW, Lee HJ, Choi JH, Koh WG, Myoung JM, Hur JH, et al. Nano Lett 2010; 10(1):347–51.
- [17] Northrup JE. Phys Rev B 2007;76(24):245202.
- [18] Henning J. J Polym Sci C 1967;16:2751–61.
- [19] Hansen D, Ho CC. J Polym Sci A: Gen Pap 1965;3(2):659–70.
- [20] Choy C. Polymer 1977;18(10):984–1004.
- [21] Kilian HG, Pietralla M. Polymer 1978;19(6):664–72.
- [22] Rantala J. Rev Sci Instrum 1992;63(11):5472–4.
- [23] Piraux L, Kinany-Alaoui M, Issi JP, Begin D, Billaud D. Solid State Commun 1989;70(4):427–9.
- [24] Choy CL, Yang GW, Wong YW. J Polym Sci B: Polym Phys 1997;35(10): 1621–31.
- [25] Kurabayashi K, Asheghi M, Touzelbaev M, Goodson KE. J Microelectromech Syst 1999;8(2):180–91.
- [26] Ju YS, Kurabayashi K, Goodson KE. Microscale Therm Eng 1998;2(2):101–10.
- [27] Ju YS, Kurabayashi K, Goodson KE. Thin Solid Films 1999;339(1–2):160–4.
- [28] Liu CJ, Oshima K, Shimomura M, Miyauchi S. Synth Met 2006;156(21–24): 1362–7.
- [29] Maizel K, Ezzahri Y, Wang X, Singer S, Majumdar A, Shakouri A. Twenty fourth annual IEEE semiconductor thermal measurement and management symposium, proceedings 2008; 2008. p. 187–92.
- [30] Wang XW, Guo JQ, Geohegan DB, Eres G, Vincent C. J Appl Phys 2008;103(11): 113505.
- [31] Feng XH, Wang XW, Chen XW, Yue YN. Acta Mater 2011;59(5):1934–44.
- [32] Feng XH, Wang XW. Thin Solid Films 2011;519(16):5700–5.
- [33] Kurabayashi K, Goodson KE. J Appl Phys 1999;86(4):1925–31.
- [34] Parker WJ, Jenkins RJ, Abbott GL, Butler CP. J Appl Phys 1961;32(9):1679–84.
- [35] Wang XW, Guo JQ, Wang T. J Appl Phys 2007;101(6):063537.
- [36] Baibarac M, Lapkowski M, Pron A, Lefrant S, Baltog I. J Raman Spectrosc 1998; 29(9):825–32.
- [37] Choy CL, Wong SP, Young K. J Polym Sci B: Polym Phys 1985;23(8):1495–504.